Energy Conversion

International Edition: DOI: 10.1002/anie.201500274
German Edition: DOI: 10.1002/ange.201500274

Dye-Controlled Interfacial Electron Transfer for High-Current Indium Tin Oxide Photocathodes**

*Zhongjie Huang, Mingfu He, Mingzhe Yu, Kevin Click, Damian Beauchamp, and Yiying Wu**

Abstract: *Efficient sensitized photocathodes are highly desired for solar fuels and tandem solar cells, yet the development is hindered by the scarcity of suitable p-type semiconductors. The generation of high cathodic photocurrents by sensitizing a degenerate n-type semiconductor (tin-doped indium oxide; ITO) is reported. The sensitized mesoporous ITO electrodes deliver cathodic photocurrents of up to 5.96 ± 0.19 mA cm^{-2}, which are close to the highest record in conventional p-type sensitized photocathodes. This is realized by the rational selection of dyes with appropriate energy alignments with ITO. The energy level alignment between the highest occupied molecular orbital of the sensitizer and the conduction band of ITO is crucial for efficient hole injection. Transient absorption spectroscopy studies demonstrate that the cathodic photocurrent results from reduction of the photoexcited sensitizer by free electrons in ITO. Our results reveal a new perspective toward the selection of electrode materials for sensitized photocathodes.*

Dye-sensitized nanoparticulate metal oxides hold great promise as photoactive electrodes for light-to-electricity conversion[1] and light-to-chemical fuels transformation.[2] In these scenarios, the efficient light absorption and charge carrier collection are highly desired and can be facilitated by suitable wide bandgap semiconductors. N-type semiconductors (n-SCs), such as TiO_2 and ZnO, have been widely used as photoanodes (Supporting Information, Figure S1a) in n-type dye-sensitized solar cells (n-DSCs),[3] perovskite solar cells,[4] and dye-sensitized photoelectrosynthesis cells (DSPECs).[2a] In contrast, the choice for the photocathode (Figure S1b) is limited. To date NiO dominates in p-DSCs and DSPECs for proton and CO_2 reduction.[5] However, the severe intrinsic problems of NiO (parasitic optical absorption and slow hole diffusion)[6] significantly limit the performance of these devices. For example, photocurrents in p-DSCs usually vary between 0.1–5.5 mA cm^{-2} (Supporting Information, Table S1),[7] with very few exceptions > 7.0 mA cm^{-2}.[8] Therefore, a novel cathode material with high optical transparency and electrical conductivity is indispensable for efficient photocathodes. Recent efforts have focused on other wide bandgap p-SCs, for example, Cu^I based delafossite complex metal oxides.[9] Nevertheless, owing to the difficulty of synthesizing small nanoparticles, progress is limited.

Tin-doped indium oxide (ITO) is a degenerate n-SC with a bandgap around 3.7–3.8 eV. Planar ITO thin film has been widely used as the transparent conductive substrate in organic photovoltaic devices[10] and organic light-emitting diodes (OLEDs).[11] Furthermore, nanostructured ITO films can serve as high-surface-area scaffolds for supporting TiO_2, hematite, photosystem II in photoelectrochemical devices,[12] and electrochemical catalysts such as water oxidation catalysts[13] and hydrogen evolution catalysts.[14]

Herein, we report the incorporation of an n-SC as an efficient photocathode in which the hole is conducted through the conduction band (CB) of the n-SC, instead of the valence band (VB) of the conventional p-SC. As a demonstration, mesoporous ITO films sensitized by energy-aligned cyclometalated ruthenium (II) complexes can generate remarkable cathodic photocurrents as high as 5.96 ± 0.19 mA cm^{-2} under one sun illumination in a DSC configuration. The superior conductivity and transparency of ITO enable the use of thick films (over 10 μm), which is a big advantage over NiO (optimal film thickness around 2–3 μm). The photocurrent generation mechanism was investigated by transient absorption spectroscopy (TAS), which demonstrated that the cathodic photocurrent results from reduction of the photoexcited sensitizer by free electrons in the CB of ITO. It should be noted that dye-sensitized ITO photoelectrodes were reported in a few instances before, but the photocurrents, either anodic or cathodic, were generally very low (below 0.05 mA cm^{-2}).[15]

Mesoporous ITO films were prepared by annealing ITO nanoparticles on fluorine-doped tin oxide (FTO) substrates at 450 °C in the air. For the sensitizer, we started with O18[16] (see Figure 1), a cyclometalated ruthenium (II) dye designed for p-DSCs. After being soaked in the O18 dye solution overnight, light-yellowish ITO films turned black, and a 11.2 μm-thick film had a transmittance of almost zero below 600 nm (Figure 2a). *J*–*V* curves of O18-sensitized ITO solar cells with I_2/LiI redox and platinized counter electrode are shown in Figure 2b. The short-circuit current density (J_{SC}) increases from 2.67 mA cm^{-2} for the cell made from a thin film (3.5 μm) to 5.96 ± 0.19 mA cm^{-2} for those from thick films with the

[*] Z. Huang,[+] M. He,[+] M. Yu, K. Click, D. Beauchamp, Prof. Y. Wu
Department of Chemistry & Biochemistry
The Ohio State University
100 West 18th Avenue, Columbus, OH 43210 (USA)
E-mail: wu@chemistry.ohio-state.edu

[+] These authors contributed equally to this work.

[**] We acknowledge support from the U.S. Department of Energy, Office of Basic Energy Sciences, Division of Materials Science and Engineering under award DE-FG02-07ER46427. Use of the Center for Nanoscale Materials was supported by the U. S. Department of Energy, Office of Science, Office of Basic Energy Sciences, under Contract No. DE-AC02-06CH11357. We appreciate the help of Dr. David Gosztola from the Center of Nanoscale Materials (CNM) of Argonne National Laboratory on transient absorption spectroscopy experiments.

Supporting information for this article is available on the WWW under http://dx.doi.org/10.1002/anie.201500274.

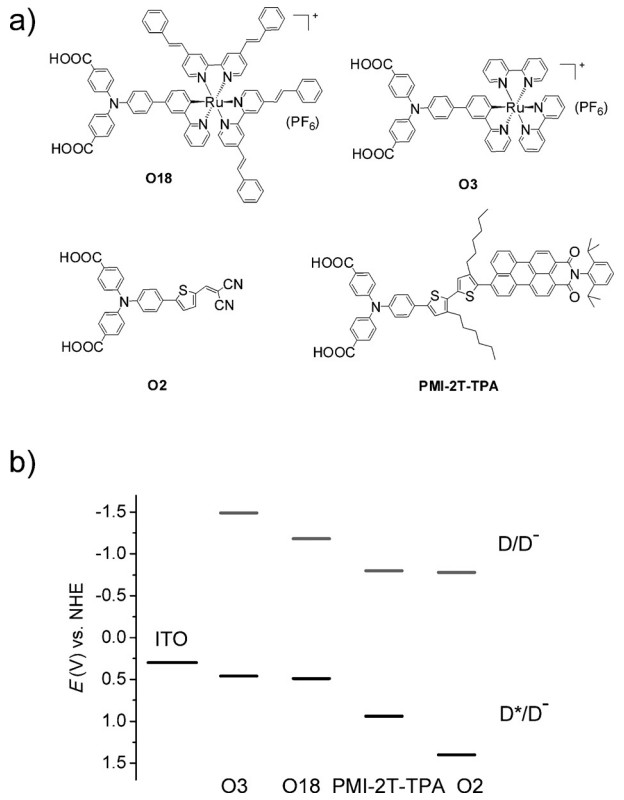

Figure 1. a) Structures of dyes used in this work; b) energy diagrams of the ITO conduction band and dyes.

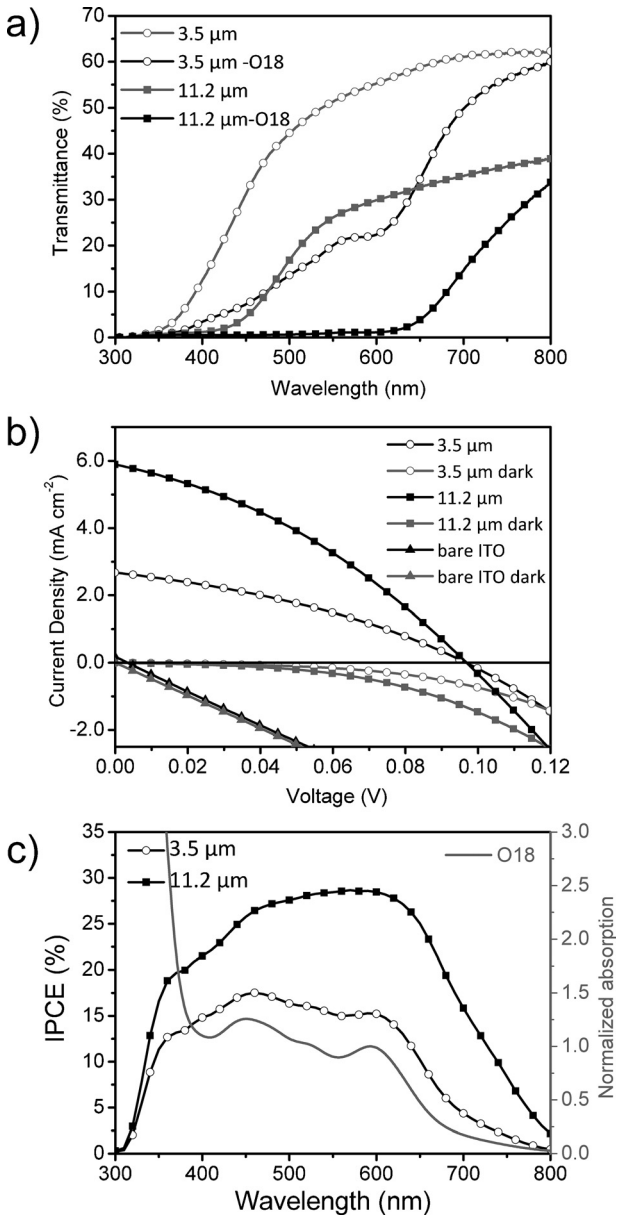

Figure 2. a) Transmittance spectra of 3.5 μm and 11.2 μm thick ITO films before (gray) and after (black) sensitization; b) *J–V* curves of O18-sensitized 3.5 μm and 11.2 μm thick ITO solar cells, and a blank ITO cell under standard one-sun illumination (black) and in the dark (gray); c) IPCE spectra of O18-sensitized 3.5 μm and 11.2 μm thick ITO films (black), and the normalized absorption spectrum of O18 in DMF (gray).

thickness of 11.1 ± 0.2 μm (data from four cells). This photocurrent density is two to three orders of magnitude higher than previously reported using sensitized ITO photoelectrodes,[15] and is close to the highest result for p-DSCs. The open-circuit voltage (V_{OC}) is around 100 mV, which is similar to dye-sensitized NiO cells with I_2/LiI redox.[16] As a control, a non-sensitized ITO cell only shows negligible V_{OC} (3 mV) and J_{SC} (0.16 mA cm^{-2}), confirming that the photovoltaic behavior comes from dye sensitization. This was further corroborated by the incident photo-to-current conversion (IPCE) measurement. IPCE spectra (Figure 2c) of two O18-sensitized ITO cells resemble the panchromatic absorption profile of O18, and the integrated currents are 2.93 and 5.77 mA cm^{-2}, respectively, which reasonably agree with the *J–V* results.

The V_{OC} of the ITO cell is comparable to that of the NiO p-DSC with the I_2/LiI redox, but lower than that of the normal TiO_2 based n-DSC. The V_{OC} is limited by the high dark current (for example 2.5 mA cm^{-2} for the 11.2 μm-thick film at 120 mV bias), which originates from the back electron transfer from I^- to ITO. This is also suggested by our investigation of the hole lifetime and transport property of ITO electrodes (Supporting Information, Figure S5). The lifetime drops exponentially with increasing voltages, leading to low charge collection efficiencies at high voltages. The current leaking from this channel can potentially be suppressed by surface blocking techniques.[17] On the other hand, the sensitized ITO photocathode has very promising applications for solar fuels, as high photovoltages are not crucial in the scenario of water and CO_2 reductions.

Furthermore, three other sensitizers (that is, O3, O2, and PMI-2T-TPA; see Figure 1 for their structures and HOMO/LUMO energetics) were investigated in this system. These dyes are all designed for efficient hole injection but with different energy levels, and their properties have been reported previously.[18] A detailed summary of their energy levels can be found in the Supporting Information, Table S2. An intriguing dye-induced photocurrent modulation/switching phenomenon was observed: the energy level of the

sensitizer can determine the photocurrent direction and magnitude on the ITO electrode. When the ITO films were maintained at 10 μm thickness, the cyclometalated ruthenium dye O3 generated a cathodic J_{SC} of 4.89 mA cm^{-2}, which performed only slightly worse than O18 (see the comparison in the Supporting Information, Figure S3). A dramatically reduced cathodic J_{SC} of 0.30 mA cm^{-2} was observed for a PMI-2T-TPA-sensitized cell, whereas the photocurrent switched direction and became anodic with J_{SC} of 0.43 mA cm^{-2} for an O2-sensitized cell.

Large cathodic photocurrents from O18 and O3-sensitized cells unambiguously demonstrate the hole transfer to the ITO electrode. However, the key question is how the ITO acts as a photoelectrode– whether the hole injection is from the excited or oxidized dye. Two possible mechanisms are illustrated in Figure 3. Mechanism I involves, as a primary

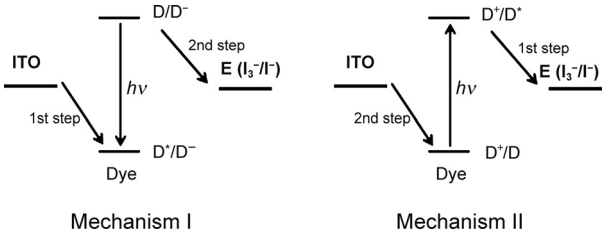

Figure 3. Illustration of two possible current-generation mechanisms.

step, hole injection from the photoexcited dye D* into CB of ITO, which is analogous to the first step in p-DSCs and DSPECs. Alternatively, the oxidative quenching of the excited dye by the electron acceptor in the electrolyte (triiodide) can occur first, followed by thermal interfacial hole transfer from the oxidized dye D^+ to ITO. We call this mechanism II, which corresponds to a typical photogalvanic cell,[19] as detailed in the Supporting Information.

TAS was used to study the charge transfer steps in both dye/ITO and dye/electrolyte interfaces. We first investigated the dye/electrolyte interface using O3 dye and triiodide. Two solutions, O3 and O3/tetrabutylammonium triiodide ($TBAI_3$), were pumped at 505 nm to selectively excite O3 and probed of the absorption change. The resulting transient difference spectra (Figure 4a) are almost identical for both solutions: the bleaching of MLCT absorption at 525–618 nm and growth of absorption at 618–750 nm, indicating the presence of identical photoexcited products. The normalized temporal absorbance changes at 556 nm of both solutions in the μs-scale are compared in Figure 4b. Their ground-state recovery kinetics can be adequately fitted with a single exponential decay equation (Supporting Information, Equation S4). The time constant is 14.3 ns for O3/$TBAI_3$ and 13.6 ns for O3. Because of the very similar kinetic processes observed in both O3 and O3/$TBAI_3$ solution, and no new spectroscopic features corresponding to charge separated species in O3/$TBAI_3$, I_3^- is unable to efficiently oxidatively quench O3*. Therefore, the likelihood of mechanism II is excluded (more discussions can be found in the Supporting Information). The photocurrent modulation should take place at the dye/ITO interface, instead of the dye/electrolyte interface.

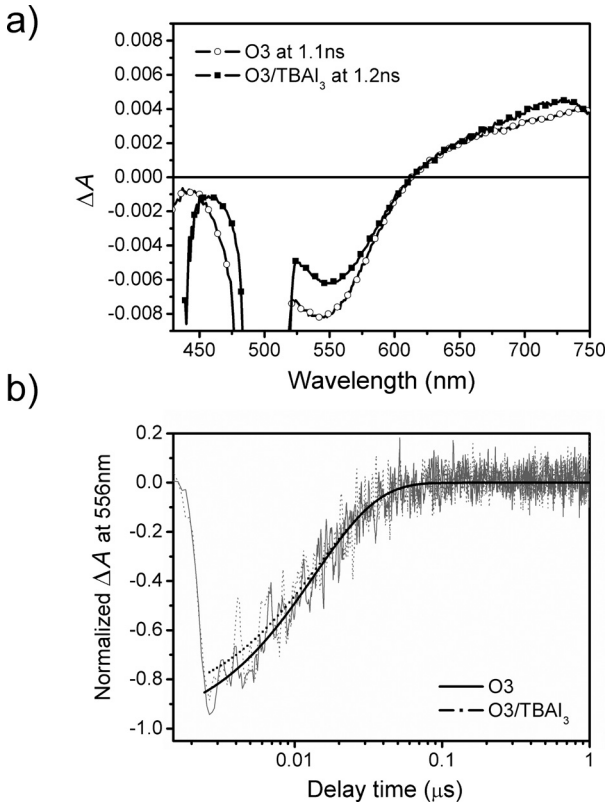

Figure 4. a) Transient difference absorption spectra of O3 and O3/$TBAI_3$ in acetonitrile; b) fitting of the normalized absorbance difference at 556 nm of O3 and O3/$TBAI_3$ in acetonitrile.

We then studied the dye/ITO interface. An O3-sensitized ITO film was excited at 505 nm and the temporal transient difference spectra are shown in Figure 5a. Within 1 ps, the ground-state bleaching from 520 to 633 nm and a growth from 633 to 750 nm were observed. Theoretically, three possible reaction pathways can exist at the dye/ITO interface upon the photoexcitation: electron injection, hole injection, and excited state decay. However, the cathodic photocurrent outputs from our O3 and O18-sensitized ITO solar cells necessitate the hole-injection process (as shown in mechanism I), since mechanism II has already been excluded. We thus attribute the ground state recovery to the geminate recombination of O3(−)/ITO(+), which is the product of the hole injection (from O3* into ITO). The ground state recovery kinetics at 558 nm was monitored and compared with that in O3 solution, as shown in Figure 5b. In O3 solution, upon excitation, the ground-state bleaching signal still maintains about 80% of the maximum values at the limit of the probe time window. This long-lived state is attributed to the O3 ^{3}MLCT state. In contrast, faster ground-state recovery is observed at the O3/ITO interface, and the kinetics can be adequately fitted with the sum of two exponential decays and a residue (Supporting Information, Equation S5). As shown in Figure 5c, two time constants, 57 ps and 1.7 ns, are obtained after the global fitting at five different wavelengths. These are the geminate recombination time constants for the O3(−)/ITO(+) charge-separated state.

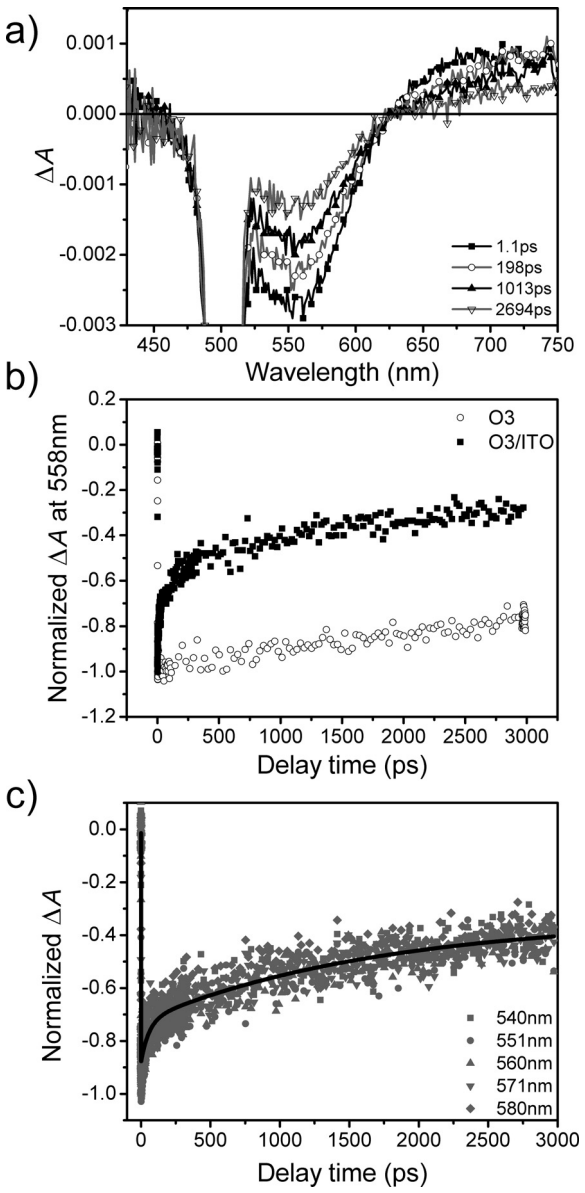

Figure 5. a) Transient difference spectra of O3/ITO at different delay time; b) normalized difference absorbance at 558 nm of O3 and O3/ITO in acetonitrile; c) global fitting of the ground-state recovery kinetics of O3/ITO at five different wavelengths.

It should be noted that the electron injection is possible at other dye/ITO interfaces. For example, at the O2/ITO interface, the formation of charge-separated O2(+)/ITO(−) is observed (Supporting Information, Figure S6) and is consistent with the anodic photocurrent outputs from our O2-sensitized ITO solar cells. Another example is a recent report of the electron-injection process in $[Ru(bpy)_2(dcb)]^{2+}$ (dcb is 4,4′-$(COOH)_2$-2,2′-bipyridyl)-sensitized nanoITO films. The electron-injection rate constant is at the order of $10^{10}\ s^{-1}$.[20] In our opinion, the lack of electron-injection process at the O3/ITO interface can be attributed to the remote location of the lowest unoccupied molecular orbital (LUMO) of O3 from ITO. LUMO of O3 is mainly localized on bpy ligands, which are far away from the ITO surface. This results in inefficient overlap of O3 LUMO with the unoccupied density of states (DOS) of ITO, as well as long electron-tunneling distance. Therefore, the electron-injection process is prohibited.

As revealed by our TAS study, photoinduced hole injection process is preferred in our Ru^{II} complex/ITO interface. We further rationalize this process in detail in Figure 6. As a degenerate semiconductor, the Fermi level of

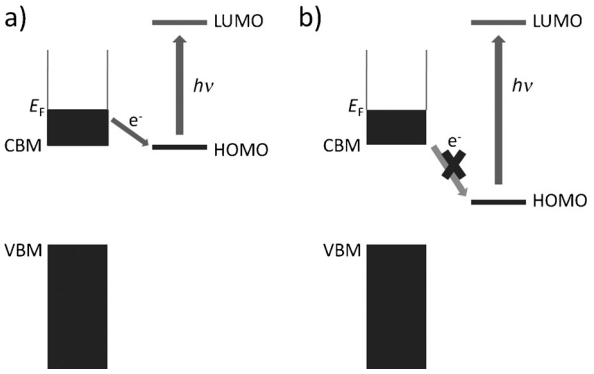

Figure 6. Working principle for dye-sensitized ITO as a photocathode: a) efficient electron transfer when energy is matched, as in O18 and O3-sensitized cells; and b) hindered electron transfer when energy is not matched, as in O2-sensitized cells.

ITO (ca. 0.2 V vs. NHE)[11] cuts through its CB, resulting in free electrons in CB and the quasi-metallic behavior. When ITO is in contact with the electrolyte, its Fermi level reaches equilibrium with the Nernst potential of the redox couple (ca. 0.3 V vs. NHE). Upon illumination, an excited dye extracts one free electron from the ITO CB (hole injection process), and the reduced dye is regenerated by the redox couple afterwards. The consumption of the electrons lowers the Fermi level of ITO and generates the positive V_{OC}.

The above mechanism indicates the importance of the energy level alignment at the ITO-sensitizer interface. According to Gerischer's interfacial electron-transfer theory,[21] efficient charge transfer at metal oxide/sensitizer interface depends critically on the overlap of the sensitizer excited-state distribution function with the DOS of the semiconductor. Efficient electron transfer occurs when the electronic acceptor level of the excited molecule has effective overlap with the ITO CB (Figure 6a). In contrast, if the HOMO of the dye is in the bandgap of ITO with minimal DOS (Figure 6b), the electron transfer is retarded. The working principle illustrated in Figure 6 explains well the dye selectivity in our cells. Figure 6a represents the cases of O18 and O3, whose HOMO (0.49 V and 0.46 V, see Figure 1b) overlaps with ITO CB. Figure 6b represents the case of O2. The HOMO of O2 (1.40 V, see Figure 1b)[18b] is much more positive than that of O18 and lies deeply in the bandgap of ITO. Its LUMO locates at −0.78 V, allowing for efficient electron injection. Along with the small anodic current ($0.43\ mA\,cm^{-2}$) observed in the *J*–*V* test, TAS studies of O2/ITO interface also confirmed the electron injection process forming charge-separated O2(+)/ITO(−) species (Support-

ing Information, Figure S5). The HOMO of PMI-2T-TPA locates at 0.94 V (Figure 1b), which is between that of O18 and O2. Therefore, a limited cathodic J_{SC} of 0.30 mA cm^{-2} was obtained.

In summary, we report an efficient dye-sensitized photocathode system by the careful design of the HOMO level of the sensitizer and the introduction of highly transparent and conductive ITO mesoporous film. As a demonstration, unprecedentedly high cathodic photocurrents from Ru^{II} complexe-sensitized mesoporous ITO films in the LiI/I_2 electrolyte have been achieved. Our TAS results confirm that the high cathodic photocurrent is attributed to the fast hole injection process from the excited dye into ITO. This novel type of photocathode can potentially break the current bottleneck and achieve wide applications in DSCs and solar fuels. Furthermore, the photocurrent direction and magnitude on ITO electrode can be modulated by tuning the HOMO level of the sensitizer.

Keywords: charge transfer · dye-sensitized solar cells · energy conversion · ruthenium · time-resolved spectroscopy

How to cite: *Angew. Chem. Int. Ed.* **2015**, *54*, 6857–6861
Angew. Chem. **2015**, *127*, 6961–6965

[1] A. Hagfeldt, G. Boschloo, L. Sun, L. Kloo, H. Pettersson, *Chem. Rev.* **2010**, *110*, 6595–6663.
[2] a) L. Alibabaei, H. Luo, R. L. House, P. G. Hoertz, R. Lopez, T. J. Meyer, *J. Mater. Chem. A* **2013**, *1*, 4133–4145; b) J. R. Swierk, T. E. Mallouk, *Chem. Soc. Rev.* **2013**, *42*, 2357–2387.
[3] B. O'Regan, M. Gratzel, *Nature* **1991**, *353*, 737–740.
[4] A. Mei, X. Li, L. Liu, Z. Ku, T. Liu, Y. Rong, M. Xu, M. Hu, J. Chen, Y. Yang, M. Grätzel, H. Han, *Science* **2014**, *345*, 295–298.
[5] a) Z. Ji, M. He, Z. Huang, U. Ozkan, Y. Wu, *J. Am. Chem. Soc.* **2013**, *135*, 11696–11699; b) A. Bachmeier, S. Hall, S. W. Ragsdale, F. A. Armstrong, *J. Am. Chem. Soc.* **2014**, *136*, 13518–13521; c) L. Li, L. Duan, F. Wen, C. Li, M. Wang, A. Hagfeldt, L. Sun, *Chem. Commun.* **2012**, *48*, 988–990.
[6] a) H. Zhu, A. Hagfeldt, G. Boschloo, *J. Phys. Chem. C* **2007**, *111*, 17455–17458; b) Z. Huang, G. Natu, Z. Ji, M. He, M. Yu, Y. Wu, *J. Phys. Chem. C* **2012**, *116*, 26239–26246.
[7] F. Odobel, L. Le Pleux, Y. Pellegrin, E. Blart, *Acc. Chem. Res.* **2010**, *43*, 1063–1071.
[8] a) S. Powar, Q. Wu, M. Weidelener, A. Nattestad, Z. Hu, A. Mishra, P. Bauerle, L. Spiccia, Y. B. Cheng, U. Bach, *Energy Environ. Sci.* **2012**, *5*, 8896–8900; b) Z. Liu, W. Li, S. Topa, X. Xu, X. Zeng, Z. Zhao, M. Wang, W. Chen, F. Wang, Y.-B. Cheng, H. He, *ACS Appl. Mater. Interfaces* **2014**, *6*, 10614–10622; c) K. A. Click, D. R. Beauchamp, B. R. Garrett, Z. Huang, C. M. Hadad, Y. Wu, *Phys. Chem. Chem. Phys.* **2014**, *16*, 26103–26111.
[9] M. Yu, T. I. Draskovic, Y. Wu, *Phys. Chem. Chem. Phys.* **2014**, *16*, 5026–5033.
[10] N. R. Armstrong, P. A. Veneman, E. Ratcliff, D. Placencia, M. Brumbach, *Acc. Chem. Res.* **2009**, *42*, 1748–1757.
[11] M. G. Helander, Z. Wang, J. Qiu, M. T. Greiner, D. P. Puzzo, Z. Liu, Z. Lu, *Science* **2011**, *332*, 944–947.
[12] a) H. W. Wang, C. F. Ting, M. K. Hung, C. H. Chiou, Y. L. Liu, Z. W. Liu, K. R. Ratinac, S. P. Ringer, *Nanotechnology* **2009**, *20*, 055601; b) S. C. Riha, B. M. Klahr, E. C. Tyo, S. Seifert, S. Vajda, M. J. Pellin, T. W. Hamann, A. B. F. Martinson, *ACS Nano* **2013**, *7*, 2396–2405; c) S. C. Riha, M. J. D. Vermeer, M. J. Pellin, J. T. Hupp, A. B. F. Martinson, *ACS Appl. Mater. Interfaces* **2013**, *5*, 360–367; d) M. Kato, T. Cardona, A. W. Rutherford, E. Reisner, *J. Am. Chem. Soc.* **2013**, *135*, 10610–10613.
[13] P. G. Hoertz, Z. Chen, C. A. Kent, T. J. Meyer, *Inorg. Chem.* **2010**, *49*, 8179–8181.
[14] N. M. Muresan, J. Willkomm, D. Mersch, Y. Vaynzof, E. Reisner, *Angew. Chem. Int. Ed.* **2012**, *51*, 12749–12753; *Angew. Chem.* **2012**, *124*, 12921–12925.
[15] a) D. Schlettwein, M. Kaneko, A. Yamada, D. Woehrle, N. I. Jaeger, *J. Phys. Chem.* **1991**, *95*, 1748–1755; b) K. E. Splan, A. M. Massari, J. T. Hupp, *J. Phys. Chem. B* **2004**, *108*, 4111–4115; c) W. Hamd, M. Chavarot-Kerlidou, J. Fize, G. Muller, A. Leyris, M. Matheron, E. Courtin, M. Fontecave, C. Sanchez, V. Artero, C. Laberty-Robert, *J. Mater. Chem. A* **2013**, *1*, 8217–8225.
[16] M. He, Z. Ji, Z. Huang, Y. Wu, *J. Phys. Chem. C* **2014**, *118*, 16518–16525.
[17] a) E. Palomares, J. N. Clifford, S. A. Haque, T. Lutz, J. R. Durrant, *J. Am. Chem. Soc.* **2003**, *125*, 475–482; b) G. A. Sewvandi, Z. Tao, T. Kusunose, Y. Tanaka, S. Nakanishi, Q. Feng, *ACS Appl. Mater. Interfaces* **2014**, *6*, 5818–5826.
[18] a) Z. Ji, G. Natu, Y. Wu, *ACS Appl. Mater. Interfaces* **2013**, *5*, 8641–8648; b) Z. Ji, G. Natu, Z. Huang, Y. Wu, *Energy Environ. Sci.* **2011**, *4*, 2818–2821; c) A. Nattestad, A. J. Mozer, M. K. R. Fischer, Y. B. Cheng, A. Mishra, P. Baeuerle, U. Bach, *Nat. Mater.* **2010**, *9*, 31–35.
[19] W. J. Albery, *Acc. Chem. Res.* **1982**, *15*, 142–148.
[20] B. H. Farnum, Z. A. Morseth, A. M. Lapides, A. J. Rieth, P. G. Hoertz, M. K. Brennaman, J. M. Papanikolas, T. J. Meyer, *J. Am. Chem. Soc.* **2014**, *136*, 2208–2211.
[21] a) D. F. Watson, G. J. Meyer, *Annu. Rev. Phys. Chem.* **2005**, *56*, 119–156; b) S. Ardo, G. J. Meyer, *Chem. Soc. Rev.* **2009**, *38*, 115–164.

Received: January 12, 2015
Revised: March 28, 2015
Published online: April 23, 2015

